Journal of Materials Chemistry

Cite this: J. Mater. Chem., 2012, 22, 14236

www.rsc.org/materials

PAPER

The effect of side-chain length on regioregular poly[3-(4-*n*-alkyl) phenylthiophene]/PCBM and ICBA polymer solar cells†

Chul-Hee Cho,‡[a] Hyeong Jun Kim,‡[a] Hyunbum Kang,[a] Tae Joo Shin[b] and Bumjoon J. Kim*[a]

Received 5th March 2012, Accepted 5th May 2012
DOI: 10.1039/c2jm31371e

The photovoltaic, charge transport, light absorption and morphology properties of a series of poly[3-(4-*n*-alkyl)phenylthiophene] (PAPT):acceptor (phenyl-C_{61}-butyric acid methyl ester (PCBM) or indene-C_{60} bisadduct (ICBA)) blend films are reported as a function of alkyl side-chain length. Regioregular poly[3-(4-*n*-butyl)phenylthiophene] (PBPT), poly[3-(4-*n*-hexyl)phenylthiophene] (PHPT), poly[3-(4-*n*-octyl)phenylthiophene] (POPT), and poly[3-(4-*n*-decyl)phenylthiophene] (PDPT) were successfully synthesized by a modified Grignard metathesis (GRIM) polymerization method. The effects of the alkyl side-chain length on the optical, electrochemical and structural properties of the polymers were carefully investigated to establish a relationship between the molecular structure and device function. Bulk heterojunction solar cells made of PAPTs blended with either PCBM or ICBA showed a strong photovoltaic property dependence on the alkyl side-chain length. Among all PAPTs used in this study, the best performance was observed in PHPT-based devices. This is the first report of the use of PHPT in polymer solar cells. In addition, PAPT devices blended with ICBA generally showed higher open-circuit voltages (V_{oc}) and power conversion efficiencies than PCBM-based devices. For example, a PHPT:ICBA photovoltaic device showed a V_{oc} of 0.79 V and a power conversion efficiency of 3.7%, which is the highest performance reported thus far using PAPT polymers. While the optical properties of PAPT/electron acceptor films exhibit the strongest effect on the short-circuit current of the devices, a balance between the optical, electrical and morphological properties of blended films caused by the alkyl side-chain length determines the overall photovoltaic performance of these devices. Therefore, our work provides a fundamental understanding of the molecular structure–device function relationship, especially with respect to changes in the alkyl side-chain length in conjugated polymers.

Introduction

Conjugated polymers, as active components in polymer solar cells (PSCs), have received great attention because of their potential for realizing large-scale, low-cost, solution fabricated and lightweight flexible devices.[1–4] Over the last decade, intensive research on PSCs has provided significant improvements in power conversion efficiency (PCE) and a better understanding of fundamental device working principles, including light absorption,[5,6] charge transport,[7,8] and blend morphology of electron donors and acceptors.[9,10] In current PSCs, blends of electron-donating conjugated polymers and electron-accepting small-molecule fullerene derivatives comprise the active layer in so-called bulk-heterojunction (BHJ) photovoltaics. In such devices, small modifications in conjugated polymer structure can induce large differences in the function of BHJ PSC devices.[11–15] In particular, a change in the alkyl solubilizing group in conjugated polymers is known to have a strong influence on physical and electrical properties, such as solubility, crystallinity, interchain packing, light absorption, electron affinity, and absorption coefficients.[16–22] In addition, even small modifications of the alkyl chain in conjugated polymers can affect their interactions with electron acceptors, resulting in dramatic changes in both the blend morphology and solar cell performance.[23–25] For example, blend of poly(3-hexylthiophene) (P3HT) and [6,6]-phenyl-C_{61}-butyric acid methyl ester (PCBM) is one of the most representative BHJ photovoltaics, with a reproducible efficiency of 4%.[26,27] However, BHJ solar cells based on regioregular poly(3-alkylthiophenes) (P3ATs) with different alkyl chain lengths have poor PCEs under the same device fabrication conditions used for P3HT-based devices.[28,29] The underlying reasons for this large dependence on P3AT side-chain length, although not fully understood, appear to be

[a]*Department of Chemical and Biomolecular Engineering, Korea Advanced Institute of Science and Technology (KAIST), Daejeon 305-701, Korea. E-mail: bumjoonkim@kaist.ac.kr; Fax: +82-42-350-3910; Tel: +82-42-350-3935*
[b]*Pohang Accelerator Laboratory, POSTECH, Pohang 790-784, Republic of Korea*

† Electronic supplementary information (ESI) available. See DOI: 10.1039/c2jm31371e

‡ These authors contributed equally to this work.

linked to changes in the light absorption and the charge mobility of thiophene polymers caused by morphological differences in solution-processed films.[30–32] Several works demonstrated that the grafting of different alkyl chains into polymer backbones can dramatically change optoelectronic properties and photovoltaic efficiency.[28,33] For example, while the use of longer and bulkier alkyl groups improves solution processibility, it also hinders intermolecular ordering and affects charge transport between polymer stacks.[34–36] In this respect, the synthesis of conjugated polymers with systematically controlled alkyl chain lengths offers a great opportunity to further optimize their photovoltaic properties and provide a fundamental understanding of the relationship between their properties and molecular structure.

Regioregular poly[3-(4-*n*-octyl)phenylthiophene] (POPT) has been shown to exhibit very promising features: a lower-lying highest occupied molecular orbital (HOMO) level, a smaller optical band gap of 1.8 eV and air stability.[37–41] Friend *et al.*[37] demonstrated a high photocurrent using a laminated bilayer POPT:poly[2-methoxy-5-(2′-ethylhexyloxy)-1,4-(1-cyano-vinylene)phenylene] (CN-PPV) device. Moreover, Fréchet *et al.*[38] reported a PCE of 2.0% in similar POPT:CN-PPV bilayer-type solar cells, which represents one of the highest reported efficiencies to date for solution-processed all-polymer solar cells. Recently, our group reported a series of POPT analogs with different side-chain densities.[41] We found that controlling the side-chain density of the POPT analogs allows tuning of their packing structure and HOMO level, thus improving the V_{oc} and PCE values. The synthetic simplicity and tunability of POPT make it very attractive for the exploration of molecular structure–device function correlations. While POPT has been used as one of the best materials for bilayer all-polymer solar cells, poly[3-(4-*n*-alkylphenyl)thiophene]s (PAPTs) with other alkyl chain lengths have not been studied to date.

In this study, we synthesized a series of PAPTs with different side-chain lengths (number of carbons in alkyl side-chain; n = 4, 6, 8, and 10) to systematically investigate the effect of the side-chain length on photovoltaic performance. We found a strong device performance dependence on the alkyl side-chain length, observing that poly[3-(4-*n*-hexylphenyl)thiophene] (PHPT) exhibited the best photovoltaic properties among PAPTs with different alkyl chain lengths. In addition, indene-C_{60}-bisadduct fullerene (ICBA) with a higher lowest unoccupied molecular orbital (LUMO) energy level than that of singly functionalized PCBM[42–46] was applied as an alternative electron-acceptor in blends with PAPTs. The PAPT:ICBA blend devices showed higher efficiency than PCBM-based devices because of a higher V_{oc}; PAPT:ICBA devices also exhibited a device performance trend as a function of alkyl chain length similar to that in PAPT:PCBM devices. For example, the PHPT:ICBA system showed the highest PCE (3.7%) among the PAPT:ICBA devices. It could be possible to establish a balance between the competing effects of solution processibility, miscibility with PCBM/ICBA, and solid-state polymer packing by tuning PAPT side-chain length. Variation in device performance as a function of side-chain length was investigated by careful characterization of the electrical, optical and morphological properties of films of four different PAPTs (n = 4, 6, 8, 10) blended with either PCBM or ICBA.

Experimental section

General procedure for the preparation of 3-(4-*n*-alkyl) phenylthiophenes (1)

To a solution of the appropriate 4-*n*-alkylbromobenzene (23.5 mmol), 2.5 mol% $Pd_2(dba)_3$, 10 mol% X-Phos and K_3PO_4 (47.0 mmol) in *n*-BuOH (50 mL), 3-thienylboronic acid (28.2 mmol) was added at room temperature. This mixture was degassed by argon bubbling, and the reaction mixture was heated at 110 °C for 12 h with vigorous stirring. Upon cooling to room temperature, the reaction mixture was extracted with hexanes (250 mL). The organic layer was washed with water (3 × 150 mL) and brine (50 mL), dried over $MgSO_4$ and concentrated *in vacuo*. The crude compound was purified by flash column chromatography using hexane as the eluent to afford the corresponding product **1**.

3-(4-Butyl)phenylthiophene (1a)

The product was obtained as a white solid (91% yield): ^{1}H NMR (500 MHz, $CDCl_3$) δ 7.52 (d, J = 8.1 Hz, 2H), 7.41–7.43 (m, 1H), 7.36–7.40 (m, 2H), 7.22 (d, J = 8.1 Hz, 2H), 2.64 (t, J = 7.7 Hz, 2H), 1.60–1.67 (m, 2H), 1.34–1.43 (m, 2H), 0.95 (t, J = 7.3 Hz, 3H).

3-(4-Hexyl)phenylthiophene (1b)

The product was obtained as a white solid (67% yield): ^{1}H NMR (500 MHz, $CDCl_3$) δ 7.51 (d, J = 8.1 Hz, 2H), 7.40–7.42 (m, 1H), 7.36–7.39 (m, 2H), 7.21 (d, J = 8.1 Hz, 2H), 2.62 (t, J = 7.7 Hz, 2H), 1.59–1.67 (m, 2H), 1.27–1.38 (m, 6H), 0.89 (t, J = 6.9 Hz, 3H).

3-(4-Octyl)phenylthiophene (1c)

The product was obtained as a white solid (82% yield): ^{1}H NMR (500 MHz, $CDCl_3$) δ 7.56 (d, J = 8.2 Hz, 2H), 7.38–7.46 (m, 3H), 7.25 (d, J = 8.2 Hz, 2H), 2.67 (t, J = 7.7 Hz, 2H), 1.66–1.73 (m, 2H), 1.27–1.45 (m, 10H), 0.95 (t, J = 6.8 Hz, 3H).

3-(4-Decyl)phenylthiophene (1d)

The product was obtained as a white solid (80% yield): ^{1}H NMR (500 MHz, $CDCl_3$) δ 7.51 (d, J = 8.2 Hz, 2H), 7.40–7.42 (m, 1H), 7.36–7.38 (m, 2H), 7.21 (d, J = 8.1 Hz, 2H), 2.62 (t, J = 7.7 Hz, 2H), 1.60–1.66 (m, 2H), 1.23–1.38 (m, 14H), 0.89 (t, J = 6.8 Hz, 3H).

General procedure for the preparation of 2-bromo-3-(4-*n*-alkyl) phenylthiophenes (2)

To a stirred solution of the appropriate 3-(4-*n*-alkyl)phenylthiophene **1** (15.0 mmol) in chloroform and acetic acid (200 mL, 3 : 1 v/v), NBS (15.75 mmol) was added at room temperature for 2 h. The reaction was monitored by TLC to establish completion. The organic layer was extracted with $CHCl_3$ (150 mL). The remaining excess NBS was removed by washing with satd aq $Na_2S_2O_3$ (50 mL), 1.0 N aq NaOH (2 × 50 mL), and water (2 × 100 mL), dried over $MgSO_4$ and concentrated *in vacuo*. The resulting crude oil product was purified by gravity column chromatography on silica gel using hexanes as the eluent to afford the corresponding product **2**.

2-Bromo-3-(4-butyl)phenylthiophene (2a)

The product was obtained as a colorless oil (89% yield): ^{1}H NMR (500 MHz, $CDCl_3$) δ 7.47 (d, $J = 8.1$ Hz, 2H), 7.29 (d, $J = 5.7$ Hz, 1H), 7.25 (d, $J = 8.4$ Hz, 2H), 7.03 (d, $J = 5.7$ Hz, 1H), 2.66 (t, $J = 7.8$ Hz, 2H), 1.61–1.68 (m, 2H), 1.36–1.44 (m, 2H), 0.96 (t, $J = 7.4$ Hz, 3H).

2-Bromo-3-(4-hexyl)phenylthiophene (2b)

The product was obtained as a colorless oil (83% yield): ^{1}H NMR (500 MHz, $CDCl_3$) δ 7.46 (d, $J = 8.1$ Hz, 2H), 7.28 (d, $J = 5.7$ Hz, 1H), 7.24 (d, $J = 8.1$ Hz, 2H), 7.02 (d, $J = 5.7$ Hz, 1H), 2.64 (t, $J = 7.7$ Hz, 2H), 1.61–1.68 (m, 2H), 1.28–1.41 (m, 6H), 0.90 (t, $J = 7.4$ Hz, 3H).

2-Bromo-3-(4-octyl)phenylthiophene (2c)

The product was obtained as a colorless oil (87% yield): ^{1}H NMR (500 MHz, $CDCl_3$) δ 7.52 (d, $J = 8.0$ Hz, 2H), 7.33 (d, $J = 5.5$ Hz, 1H), 7.29 (d, $J = 8.5$ Hz, 2H), 7.07 (d, $J = 5.5$ Hz, 1H), 2.69 (t, $J = 7.5$ Hz, 2H), 1.66–1.73 (m, 2H), 1.24–1.45 (m, 10H), 0.95 (t, $J = 6.8$ Hz, 3H).

2-Bromo-3-(4-decyl)phenylthiophene (2d)

The product was obtained as a colorless oil (83% yield): ^{1}H NMR (500 MHz, $CDCl_3$) δ 7.47 (d, $J = 8.2$ Hz, 2H), 7.29 (d, $J = 5.7$ Hz, 1H), 7.24 (d, $J = 8.1$ Hz, 2H), 7.03 (d, $J = 5.7$ Hz, 1H), 2.64 (t, $J = 7.7$ Hz, 2H), 1.61–1.69 (m, 2H), 1.23–1.40 (m, 14H), 0.88 (t, $J = 6.8$ Hz, 3H).

General procedure for the preparation of 2-bromo-5-iodo-3-(4-*n*-alkyl)phenylthiophenes (3)

To a stirred solution of the appropriate 2-bromo-3-(4-*n*-alkyl) phenylthiophene **2** (12.0 mmol) in chloroform and acetic acid (160 mL, 3 : 1 v/v), *N*-iodosuccinimide (NIS) (14.4 mmol) was added, and the mixture was warmed and stirred at 60 °C for 10 h. The reaction was monitored by TLC to establish completion. The excess NIS was removed by washing with saturated aq $Na_2S_2O_3$ (100 mL). The organic layer was extracted with $CHCl_3$ (120 mL), washed with 1.0 N aq NaOH (2 × 40 mL) and water (2 × 100 mL), dried over $MgSO_4$ and concentrated *in vacuo*. The resulting crude product was purified by gravity column chromatography on silica gel using hexanes as the eluent to afford the corresponding product **3**.

2-Bromo-5-iodo-3-(4-butyl)phenylthiophene (3a)

The product was obtained as a pale yellow oil (81% yield): ^{1}H NMR (500 MHz, $CDCl_3$) δ 7.40 (d, $J = 8.1$ Hz, 2H), 7.23 (d, $J = 8.1$ Hz, 2H), 7.18 (s, 1H), 2.64 (t, $J = 7.8$ Hz, 2H), 1.58–1.67 (m, 2H), 1.33–1.43 (m, 2H), 0.95 (t, $J = 7.4$ Hz, 3H).

2-Bromo-5-iodo-3-(4-hexyl)phenylthiophene (3b)

The product was obtained as a pale yellow oil (78% yield): ^{1}H NMR (500 MHz, $CDCl_3$) δ 7.41 (d, $J = 8.2$ Hz, 2H), 7.24 (d, $J = 8.2$ Hz, 2H), 7.19 (s, 1H), 2.65 (t, $J = 7.7$ Hz, 2H), 1.62–1.69 (m, 2H), 1.28–1.42 (m, 6H), 0.91 (t, $J = 7.2$ Hz, 3H).

2-Bromo-5-iodo-3-(4-octyl)phenylthiophene (3c)

The product was obtained as a pale yellow oil (84% yield): ^{1}H NMR (500 MHz, $CDCl_3$) δ 7.44 (d, $J = 8.0$ Hz, 2H), 7.26 (d, $J = 8.0$ Hz, 2H), 7.22 (s, 1H), 2.68 (t, $J = 8.0$ Hz, 2H), 1.64–1.72 (m, 2H), 1.25–1.45 (m, 10H), 0.94 (t, $J = 7.0$ Hz, 3H).

2-Bromo-5-iodo-3-(4-decyl)phenylthiophene (3d)

The product was obtained as a pale yellow oil (83% yield): ^{1}H NMR (500 MHz, $CDCl_3$) δ 7.40 (d, $J = 8.1$ Hz, 2H), 7.23 (d, $J = 8.1$ Hz, 2H), 7.19 (s, 1H), 2.63 (t, $J = 7.8$ Hz, 2H), 1.61–1.67 (m, 2H), 1.22–1.40 (m, 14H), 0.89 (t, $J = 7.0$ Hz, 3H).

General procedure for the synthesis of poly[3-(4-*n*-alkyl) phenylthiophene] (PAPT)

A dry 250 mL two-neck flask was flashed with argon and was charged with 2-bromo-5-iodo-3-(4-*n*-alkyl)phenylthiophene **3** and anhydrous THF (0.05 M conc). The resulting solution was cooled to −78 °C and stirred for 0.5 h. Then, *i*-PrMgCl (2.0 M in THF, 0.95 equiv.) was added to the reaction mixture dropwise. Then, after stirring at −78 °C for 1 h, the reaction mixture was allowed to cool to room temperature, and then 0.3 mol% Ni(dppp)Cl_2 was added to the reaction mixture. After 12 h at 65 °C, the polymer was precipitated into methanol from the THF solution and filtered through a Soxhlet thimble. The polymer was isolated from the solvent fraction, followed by precipitation into methanol. The polymer was dried under vacuum to give the desired PAPT polymer.

Poly[3-(4-n-butyl)phenylthiophene] (PBPT) was prepared by the reaction of 2-bromo-5-iodo-3-(4-*n*-butyl)phenylthiophene **3a** (1.0 g, 2.38 mmol) and THF (100 mL) with *i*-PrMgCl (2.0 M in THF, 1.13 mL, 2.26 mmol) in the presence of Ni(dppp)Cl_2 (0.3 mol%, 3.9 mg) at the reflux temperature instead of 65 °C with more dilute condition (≈ 0.025 M conc.). This compound was prepared according to a modified general procedure. The desired polymer was isolated by precipitation into methanol and purified by Soxhlet extraction using methanol, acetone, hexane, chloroform and chlorobenzene as solvents. The polymer was dried under vacuum to give a black solid with metallic luster (110 mg, 21.4%): ^{1}H NMR (500 MHz, $CDCl_3$) δ 7.21 (d, $J = 7.8$ Hz, 2H), 7.15 (d, $J = 7.8$ Hz, 2H), 6.77 (s, 1H), 2.62 (t, $J = 7.6$ Hz, 2H), 1.55–1.65 (m, 2H), 1.27–1.43 (m, 2H), 0.86 (t, $J = 7.2$ Hz, 3H); $M_n = 10.3$ kg mol^{-1}, PDI = 1.94.

Poly[3-(4-n-hexyl)phenylthiophene] (PHPT) was prepared by the reaction of 2-bromo-5-iodo-3-(4-*n*-hexyl)phenylthiophene **3b** (838 mg, 1.87 mmol) and THF (38 mL) with *i*-PrMgCl (2.0 M in THF, 0.89 mL, 1.78 mmol) in the presence of Ni(dppp)Cl_2 (0.3 mol%, 3.1 mg). The desired polymer was isolated by precipitation into methanol and purified by Soxhlet extraction using methanol, acetone, hexane, chloroform and chlorobenzene as solvents. The polymer was dried under vacuum to give a black solid with metallic luster (171 mg, 37.4%): ^{1}H NMR (500 MHz, $CDCl_3$) δ 7.22 (d, $J = 8.0$ Hz, 2H), 7.15 (d, $J = 8.0$ Hz, 2H), 6.78 (s, 1H), 2.61 (t, $J = 7.6$ Hz, 2H), 1.55–1.65 (m, 2H), 1.20–1.38 (m, 6H), 0.86 (t, $J = 6.8$ Hz, 3H); $M_n = 22.4$ kg mol^{-1}, PDI = 1.98.

Poly[3-(4-n-octyl)phenylthiophene] (POPT) was prepared by the reaction of 2-bromo-5-iodo-3-(4-*n*-octyl)phenylthiophene **3c** (1.0 g, 2.10 mmol) and THF (42 mL) with *i*-PrMgCl (2.0 M in

THF, 1.0 mL, 1.99 mmol) in the presence of Ni(dppp)Cl_2 (0.3 mol%, 3.4 mg). The desired polymer was isolated by precipitation into methanol and purified by Soxhlet extraction using methanol, acetone, hexane, chloroform and chlorobenzene as solvents. The polymer was dried under vacuum to give a black solid with metallic luster (244 mg, 42.7%): ^{1}H NMR (500 MHz, $CDCl_3$) δ 7.23 (d, $J = 8.0$ Hz, 2H), 7.15 (d, $J = 8.0$ Hz, 2H), 6.79 (s, 1H), 2.61 (t, $J = 7.6$ Hz, 2H), 1.52–1.65 (m, 2H), 1.15–1.40 (m, 10H), 0.87 (t, $J = 6.7$ Hz, 3H); $M_n = 22.0$ kg mol^{-1}, PDI = 1.74.

Poly[3-(4-n-decyl)phenylthiophene] (PDPT) was prepared by the reaction of 2-bromo-5-iodo-3-(4-*n*-decyl)phenylthiophene **3d** (1.12 g, 2.22 mmol) and THF (45 mL) with *i*-PrMgCl (2.0 M in THF, 1.06 mL, 2.11 mmol) in the presence of Ni(dppp)Cl_2 (0.3 mol%, 3.6 mg). The desired polymer was isolated by precipitation into methanol and purified by Soxhlet extraction using methanol, acetone, hexane, and chloroform as solvents. The polymer was dried under vacuum to give a black solid with metallic luster (76 mg, 11.4%): ^{1}H NMR (500 MHz, $CDCl_3$) δ 7.22 (d, $J = 8.2$ Hz, 2H), 7.15 (d, $J = 8.2$ Hz, 2H), 6.78 (s, 1H), 2.61 (t, $J = 7.6$ Hz, 2H), 1.58–1.68 (m, 2H), 1.15–1.40 (m, 14H), 0.87 (t, $J = 7.0$ Hz, 3H); $M_n = 7.9$ kg mol^{-1}, PDI = 1.82.

Characterization methods

UV-visible absorption spectra were obtained with a JASCO V-570 spectrophotometer. The blend morphology of the active layer PAPT:PCBM and PAPT:ICBA blend films was examined by atomic force microscopy (AFM) (Veeco Dimension 3100) in tapping mode. Different samples (PBPT:PCBM, PHPT:PCBM, POPT:PCBM, PDPT:PCBM, PBPT:ICBA, PHPT:ICBA, POPT:ICBA and PDPT:ICBA) were prepared on a PEDOT:PSS/Si substrate for device fabrication (1 : 0.7, w/w). Grazing incidence X-ray diffraction (GIXRD) measurements were performed at beamline 9A in the Pohang Accelerator Laboratory (South Korea). X-rays with a wavelength of 1.1010 Å were used. The incidence angle (~0.15°) was chosen to allow for complete penetration of X-rays into the polymer film. The scattering spectra were collected as a 2D image map that can be divided into a component in the plane of the substrate (q_{xy}) and a component perpendicular to the substrate (q_z).

Devices fabrication and measurement

BHJ PSC cells were fabricated using an ITO/PEDOT:PSS/PAPT:acceptor/LiF/Al structure. PAPTs (PBPT, PHPT, POPT and PDPT) were used as electron donors and either PCBM or ICBA was used as the electron acceptor. ITO-coated glass substrates were ultrasonicated in acetone and 2% Helmanex soap in water, extensively rinsed with deionized water, then ultrasonicated in deionized water and isopropyl alcohol. Finally, the substrates were dried for several hours in an oven at 80 °C. The ITO substrates were treated with UV-ozone prior to PEDOT:PSS deposition. A filtered dispersion of PEDOT:PSS in water (PH 500) was applied by spin-coating at 3000 rpm for 40 s and baking for 30 min at 140 °C in air. After application of the PEDOT:PSS layer, all subsequent procedures were performed in a glove box under a N_2 atmosphere. Separate solutions of PBPT, PHPT, POPT, PDPT, PCBM and ICBA in *o*-DCB (30 mg mL^{-1}) were prepared and stirred at 120 °C for at least 24 h before being filtered through a 0.45 μm PTFE syringe filter. Blend solutions composed of PBPT, PHPT, POPT and PDPT mixed with PCBM or ICBA were prepared to a final PAPT concentration of 14 mg mL^{-1}. Each solution was spin-cast onto an ITO/PEDOT:PSS substrate at 900 rpm for 40 s. The substrates were then placed in an evaporation chamber and held under high vacuum (below 10^{-1} Torr) for at least 1 h before deposition of approximately 0.7 nm of LiF and 100 nm of Al with a shadow mask that produced four independent devices on each substrate. Then, all PAPT:PCBM and ICBA devices were thermally annealed at 180 °C for 2 min. The photovoltaic performance of the devices was characterized with an air-mass (AM) 1.5 G filter. The intensity of the solar simulator was carefully calibrated using an AIST-certified silicon photodiode. Current–voltage behavior was measured using a Keithley 2400 SMU. The active area of the fabricated devices was 0.102 cm^2. The hole mobilities of the PAPT:PCBM and PAPT:ICBA blended systems were measured by the SCLC method using an ITO/PEDOT:PSS/blend/Au device structure. The SCLC is described by:

$$J_{SCLC} = \frac{9}{8}\varepsilon\varepsilon_0\mu\frac{V^2}{L^3}$$

where ε_0 is the permittivity of free space, ε is the dielectric constant of the polymer, μ is the charge carrier mobility, V is the potential across the device ($V = V_{applied} - V_{bi} - V_r$), and L is the polymer layer thickness. The series and contact resistances of the device (~25 Ω) were measured using a blank device (ITO/PEDOT:PSS/Au), and the voltage drop caused by this resistance (V_r) was subtracted from the applied voltage.

Results and discussion

The chemical structure of the PAPTs and fullerene acceptors is shown in Fig. 1. PAPT side-chain length increases in the order PBPT, PHPT, POPT, and PDPT according to the number of carbon atoms in the alkyl chain, $n = 4$, 6, 8 and 10, respectively.

Scheme 1 presents the synthesis of four types of PAPTs containing different alkyl chains at the *para* position on the phenyl ring. The appropriate precursors, 2-bromo-5-iodo-3-(4-*n*-alkyl) phenylthiophenes **3a–d**, were obtained by a three-step synthetic path *via* successive Suzuki–Miyaura coupling, regioselective bromination, and iodination. The key steps in the monomer synthesis are bromination and iodination at the 2- and 5-positions, respectively, of the 3-(4-*n*-alkyl)phenylthiophenes **1a–d**. Compounds **1–3** were successfully prepared and identified by ^{1}H NMR spectroscopy (Schemes S1–S4†). Then, the desired PAPT polymers with different alkyl chain lengths (*i.e.*, PBPT, PHPT, POPT, and PDPT) were obtained by a modified Grignard metathesis (GRIM) polymerization at 65 °C.[37,47] The monomers used here were 2-bromo-5-iodo-3-(4-butyl)phenylthiophene **3a**, 2-bromo-5-iodo-3-(4-hexyl)phenylthiophene **3b**, 2-bromo-5-iodo-3-(4-octyl)phenylthiophene **3c**, and 2-bromo-5-iodo-3-(4-decyl)phenylthiophene **3d**, which have good selectivity for activation by isopropylmagnesium chloride and subsequent polymerization *via* nickel catalyst.

The number-average molecular weight (M_n) and polydispersity index (PDI) of the obtained polymers were analyzed by high-temperature size-exclusion chromatography (SEC) calibrated with polystyrene standards using UV and RI detectors

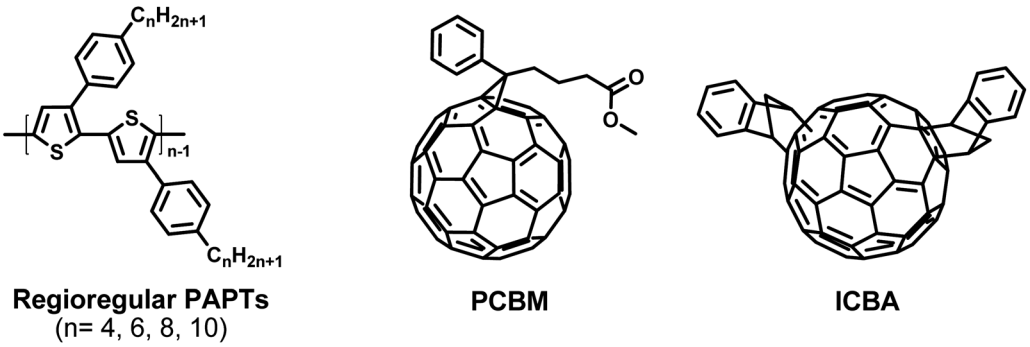

Fig. 1 Molecular structure of regioregular PAPTs and fullerene acceptors (PCBM and ICBA) used in this study.

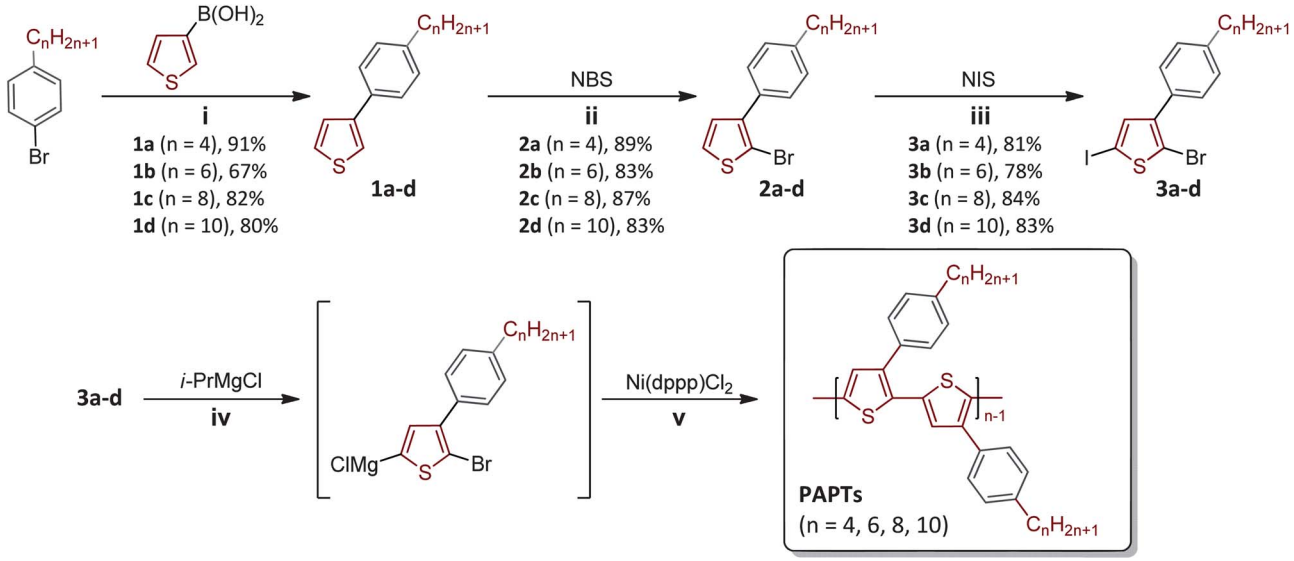

Scheme 1 Synthetic route for different alkyl side-chain-containing regioregular PAPTs. *Reaction conditions*: (i) 2.5 mol% $Pd_2(dba)_3$, 10 mol% X-Phos, K_3PO_4 (2.0 equiv.), *n*-BuOH (0.5 M conc.), 3-thienylboronic acid (1.2 equiv.), 80 °C, 12 h. (ii) NBS (1.05 equiv.), AcOH : $CHCl_3$ (1 : 3, v/v), rt, 2 h. (iii) NIS (1.2 equiv.), AcOH : $CHCl_3$ (1 : 3, v/v), 60 °C, 10 h. (iv) *i*-PrMgCl (0.95 equiv.), THF, −78 °C to rt, 1.5 h. (v) 0.3 mol% Ni(dppp)Cl_2, 65 °C, 20 h.

(Table S1†). The polymerization conditions, including reaction time and concentration, were carefully controlled to produce similar M_n and PDI values for different PAPTs. The M_n of all polymers ranged from 10 to 20 kg mol^{-1}, with a PDI of 1.7–2.0, and all polymers were found to have high regioregularity (>99%), as determined by ^1H NMR (Scheme S5†).

Grazing incidence X-ray diffraction (GIXRD) patterns of the four regioregular PAPTs are shown in Fig. 2. A thin layer (20–30 nm) of PEDOT:PSS was spin-coated onto silicon substrates followed by the polymer layer on top; the substrates were then thermally annealed at 180 °C for 1 h. Fig. 2(a)–(d) show the GIXRD patterns of PBPT, PHPT, POPT and PDPT, respectively; each of the 2D GIXRD pattern images can be divided into a component in the plane of the substrate ($\boldsymbol{q}_{xy}$) and a component perpendicular to the substrate ($\boldsymbol{q}_z$). In all four samples, the diffraction peaks were strongest in the out-of-plane direction, indicating that the polymer films had a well-organized structure with lamellar conjugated polymer stacks oriented along the perpendicular axis of the substrate. The interlayer domain spacings of PBPT, PHPT, POPT and PDPT calculated from the $\boldsymbol{q}_{xy}$ values of GIXRD patterns were 2.15, 2.51, 2.99 and 3.31 nm, respectively, indicating that the distance between adjacent PAPT

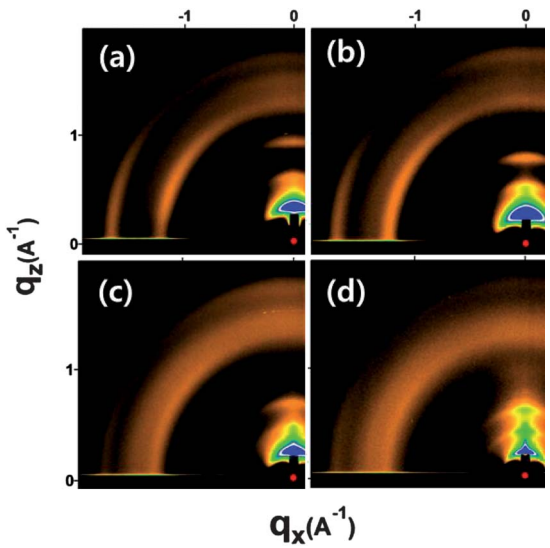

Fig. 2 GIXRD images of (a) PBPT, (b) PHPT, (c) POPT, and (d) PDPT thin films after annealing for 1 h at 180 °C.

lamellae increased by approximately 0.4 nm with the addition of two carbons to the alkyl chains. Longer side-chains resulted in larger interlayer spacings, clearly indicating that the planar thiophene backbone stacks were uniformly spaced by the phenyl-alkyl side-chains. A similar trend was observed in poly(3-alkylthiophene) (P3AT) systems; regioregular P3ATs (P3BT, P3HT, P3OT, and P3DT) showed that the interlayer domain spacing increased by approximately 0.4 nm with the addition of two carbons to the alkyl side-chain (*i.e.*, from P3HT to POPT, from P3OT to P3DT).[16] PHPT ($n = 6$) shows a significantly higher domain spacing than P3HT (2.51 *vs.* 1.65 nm), which has the same number of carbons in the alkyl side-chain.[48–50] The increased domain spacing by 0.86 nm is due to the presence of bulky phenyl rings between the alkyl side-chain and thiophene ring in PHPT. Moreover, for a given number of carbons in the alkyl chain, the difference in interlayer domain spacing between PAPTs and P3ATs is found to be constant at approximately 0.9 nm.[29]

To provide some general insight into the polymer packing structure, high resolution bulk X-ray diffraction (XRD) patterns were also measured for the four different regioregular PAPTs. XRD patterns were normalized with respect to the peak at $q = 1.25$ Å^{-1} and plotted in Fig. 3. The PAPT diffraction features centered at $q = 1.25$ and 1.70 Å^{-1} correspond to spacings of 0.38 and 0.51 nm, respectively. The numbers, which are independent of side-chain length, can be attributed to the π–π stacking distance between PAPT chains. The presence of two peaks at 0.38 and 0.51 nm suggests the presence of two different π–π stacking distances in PAPTs, which is consistent with a report by Fréchet *et al.* on POPT polymers.[39]

These two different π–π stacking distances arise from the two major phenyl ring conformations relative to the PAPT backbone: the π–π stacking distance of 0.51 nm corresponds to an orientation of the phenyl ring perpendicular to the backbone, while that at 0.38 nm corresponds to a parallel phenyl ring. The twisted phenyl ring causes an increase in distance between adjacent polymer chains. Interestingly, whereas the 0.38 and 0.51 nm peak intensities were constant regardless of the alkyl chain length, the intensity of the shoulder intermediate between the two peaks increased as the alkyl chain length increased. This finding

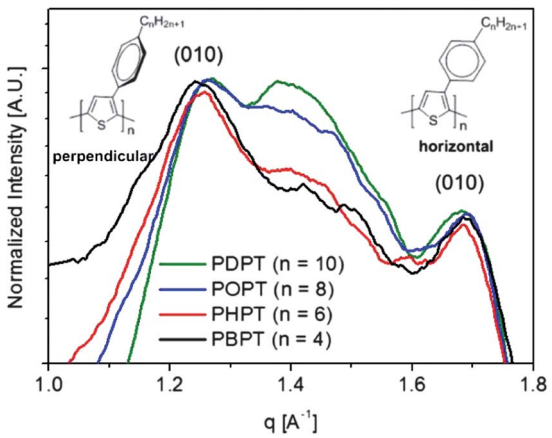

Fig. 3 Normalized XRD patterns of regioregular PAPT films. Two different (010) peaks at $q = 1.25$ and 1.7 Å^{-1} indicate two major conformations of POPT polymers, where phenyl rings are either flat or twisted perpendicular relative to the backbone.

indicates that a longer and thus more flexible alkyl chain can better accommodate the twisted phenyl conformation. In general, π–π stacking is critical for both charge transport and light absorption in conjugated polymers.[51,52] The phenyl ring torsion can induce different intermolecular interactions that lead to different optoelectronic properties.

Fig. 4(a) and (b) show current density *versus* voltage (*J–V*) curves of the ITO/PEDOT:PSS/PAPT:electron acceptors ((a) PCBM or (b) ICBA)/LiF/Al devices under AM 1.5 illumination at 100 mW cm^{-2}. The PAPT:PCBM blend solutions in *o*-dichlorobenzene (*o*-DCB) were filtered and spin-coated on ITO/glass substrates covered by a PEDOT:PSS layer. PBPT, because of its short alkyl chain, has very limited solubility even in hot *o*-DCB; for this reason, PBPT-based solar cell devices were fabricated without filtration. Optimized devices with a 1 : 0.7 w/w PAPT:acceptor weight ratio had active layer thicknesses between 80 and 100 nm and were annealed for 2 min at 180 °C. Photovoltaic performances are summarized in Table 1. The PCE of the POPT:PCBM device was 2.13% ($V_{oc} = 0.51$ V, $J_{sc} = 8.25$ mA cm^{-2}, FF = 0.50), which agrees well with previous findings.[38,41] Among the PAPT:PCBM-based BHJ PSCs, the PHPT:PCBM device exhibited the highest PCE of 2.51% ($V_{oc} = 0.48$ V, $J_{sc} = 9.73$ mA cm^{-2}, and FF = 0.53). We observed a nonlinear device performance dependence on the alkyl chain length, increasing in the order of PDPT, PBPT, POPT and PHPT. To gain insight into the effect of different alkyl chain lengths on photovoltaic properties, we also fabricated solar cells using ICBA as an electron acceptor, which has a higher LUMO energy level than PCBM and thus provides a higher V_{oc}. A similar photovoltaic performance trend with respect to alkyl side-chain length was observed in PAPT:ICBA devices, increasing in the order of PDPT, PBPT, POPT and PHPT. Note that the PHPT:ICBA device exhibited the highest PCE value among all PAPT-based BHJ devices, 3.73% (V_{oc}: 0.78 V, J_{sc}: 9.60 mA cm^{-2}, and FF: 0.50). The essential device parameters (V_{oc}, J_{sc}, FF and PCE) of the PAPT:PCBM and PAPT:ICBA systems are compared in Fig. 5. PAPT devices with ICBA as an electron acceptor exhibited higher performances than devices based on PAPT:PCBM blends. The increase in PCE was largely caused by an increase in V_{oc}; increases of more than 0.2–0.25 V over those of the PAPT:PCBM devices were observed (PBPT: 0.45 to 0.73 V, PHPT: 0.48 to 0.78 V, POPT: 0.51 to 0.78 V, and PDPT: 0.57 to 0.79 V). Interestingly, the increase in V_{oc} is more pronounced for PAPTs with a shorter alkyl chain length. For example, while the increase in V_{oc} for PDPT:ICBA over that of PDPT:PCBM was 0.22 V, the V_{oc} increase was 0.3 V for the PHPT-based devices. The enhancement in the V_{oc} and device performance observed in this study agrees well with previous reports regarding P3HT:ICBA systems.[42,43] Due to higher-lying LUMO levels than PCBM, bisadduct-type fullerenes including ICBA show potential for replacing PCBM. However, the increase in PCE has been limited to P3HT-based systems.[53,54] Therefore, our results suggest that bisadduct-type fullerenes can be applied as electron acceptors to achieve enhanced V_{oc} and PCE values in non-P3HT-based systems.

Interestingly, the V_{oc} of PAPT-based BHJ devices increased gradually with increasing PAPT alkyl chain length. In particular, the PAPT:PCBM systems showed V_{oc} values ranging from 0.45 V (PBPT) to 0.57 V (PDPT). Despite the linear trend in V_{oc},

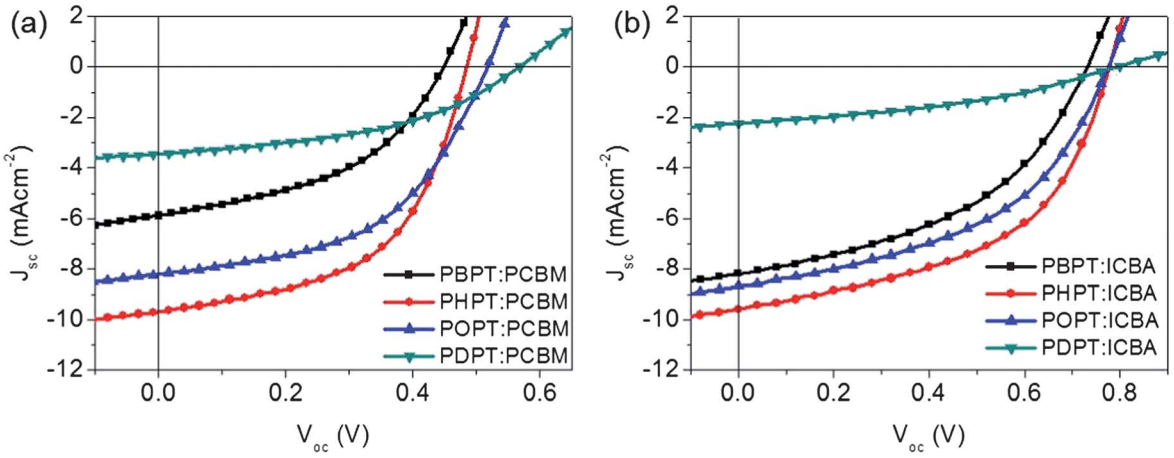

Fig. 4 Current density–voltage (J–V) characteristics of BHJ PSCs based on blends of PAPTs (PBPT, PHPT, POPT and PDPT) as donors with two types of acceptors ((a) PCBM or (b) ICBA) under AM 1.5 G simulated solar illumination (100 mW cm^{-2}). The weight ratio of electron donor to acceptor was kept constant (1 : 0.7 w/w).

Table 1 Device characteristics of BHJ PSCs composed of PAPT:electron acceptor (PCBM or ICBA) blends under AM 1.5 G simulated solar illumination (100 mW cm^{-2})

Active layer	V_{oc} (V)	J_{sc} (mA cm^{-2})	FF	PCE (%)
PBPT:PCBM	0.45	5.88	0.45	1.19
PHPT:PCBM	0.48	9.73	0.53	2.51
POPT:PCBM	0.51	8.25	0.50	2.13
PDPT:PCBM	0.57	3.38	0.44	0.85
PBPT:ICBA	0.73	8.18	0.45	2.67
PHPT:ICBA	0.78	9.60	0.50	3.73
POPT:ICBA	0.78	8.67	0.47	3.16
PDPT:ICBA	0.79	2.24	0.38	0.67

PHPT-based devices showed the highest efficiencies because of their much higher J_{sc} and FF values (Fig. 5(b) and (d)). It was observed that the dramatic changes in PCE of the PAPT:acceptor devices upon altering the alkyl side-chain length were due to the large differences in J_{sc} and FF values. For example, the PDPT:ICBA device, which has the highest V_{oc} value (V_{oc} = 0.79 V) of the four PAPT:ICBA devices, suffered from low current density (J_{sc} = 2.24 mA cm^{-2}) and low PCE (0.67%).

To better understand the effect of alkyl side-chain length on the electrical properties of PAPT solar cells, the space-charge-limited current (SCLC) of hole-only devices was measured and analyzed (Fig. S2†). The SCLC mobility measures hole mobility in the direction perpendicular to the electrodes and is thus the most reasonable measurement of the electrical properties of PAPTs in blend films. Hole-only devices were constructed under optimized device conditions, with the structure of ITO/PEDOT:PSS/PAPT:acceptor/Au (using either PCBM or ICBA as the acceptor material) and hole mobilities were calculated using the Mott–Gurney equation. Whereas PAPT:PCBM BHJ photovoltaic devices showed very different J_{sc} values, ranging from 3.38 to 9.73 mA cm^{-2} (PDPT and PHPT, respectively), no significant differences between the devices were found in the hole mobilities. Hole mobilities were in the range of 1.86×10^{-4} to 4.57×10^{-4} cm^2 V^{-1} s^{-1} for PAPT:PCBM devices and 1.27×10^{-4} to 1.90×10^{-4} cm^2 V^{-1} s^{-1} for PAPT:ICBA devices (Table S2†). The measured mobility value for the POPT:PCBM device (2.98×10^{-4} cm^2 V^{-1} s^{-1}) agrees well with that reported previously in the literature.[38,40]

The light absorption of the active layer is one of the major factors affecting the J_{sc} values of PSC devices. Fig. 6 shows the thin film optical absorption spectra of (a) PAPT:PCBM and (b) PAPT:ICBA blend films, each of which was constructed under conditions affording the most efficient devices. The optical properties of the blend films are summarized in Table 2. The optical absorption spectra of the PAPT:acceptor films display three maxima in the 500–700 nm range but show significant differences in peak location and relative peak intensities with changing alkyl chain length. The spectra of PHPT:acceptor films showed the strongest red-shift of the PAPT devices, with the maximum absorption (λ_{max}) found at 603 nm for PHPT:PCBM and 604 nm for PHPT:ICBA (Table 2). The λ_{max} values of POPT blend films are slightly blue-shifted relative to those of PHPT blends; POPT:PCBM and POPT:ICBA showed maximum absorption at 601 and 600 nm, respectively. PBPT showed further blue-shifted absorption spectra, showing maximum absorption at approximately 596 nm for PBPT:PCBM devices and 598 nm for PBPT:ICBA devices. PDPT showed a more dramatic blue-shift in absorption spectra (λ_{max} = 588 nm for PDPT:PCBM and λ_{max} = 587 nm for PDPT:ICBA). This blue-shift indicates weaker intermolecular ordering between conjugated polymers; conversely, the strong red-shift of PHPT absorption features indicates a significantly higher degree of ordering in PHPT polymers compared with PBPT and POPT polymers, which is among the reasons for improved solar-cell performance. In addition to differences in the location of the maximum absorption peak, the optical spectra of the PAPT:PCBM and PAPT:ICBA films exhibited different intensities for the λ_{max} and vibronic peaks at 600 and 650 nm, respectively. The vibronic peak at ~650 nm is a unique characteristic of highly ordered PAPT chains.[38,40,41] The absorption spectra of PAPT:PCBM and PAPT:ICBA blends were normalized with respect to the first absorption peak at approximately 550 nm; the relative intensities of the λ_{max} peak at ~600 nm (I_{max}/I_{1st}) and the vibronic peak at ~650 nm (I_{vib}/I_{1st}), compared

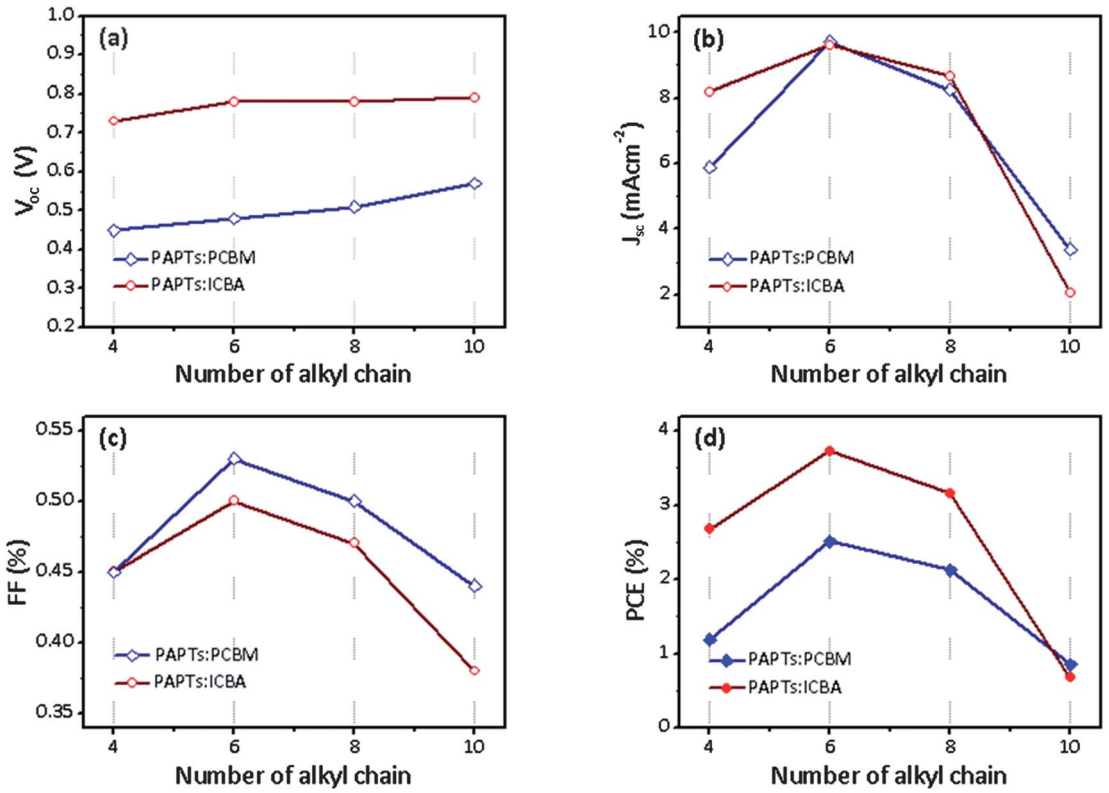

Fig. 5 Variation of key solar cell parameters ((a) V_{oc}, (b) J_{sc}, (c) FF and (d) PCE) with alkyl chain length.

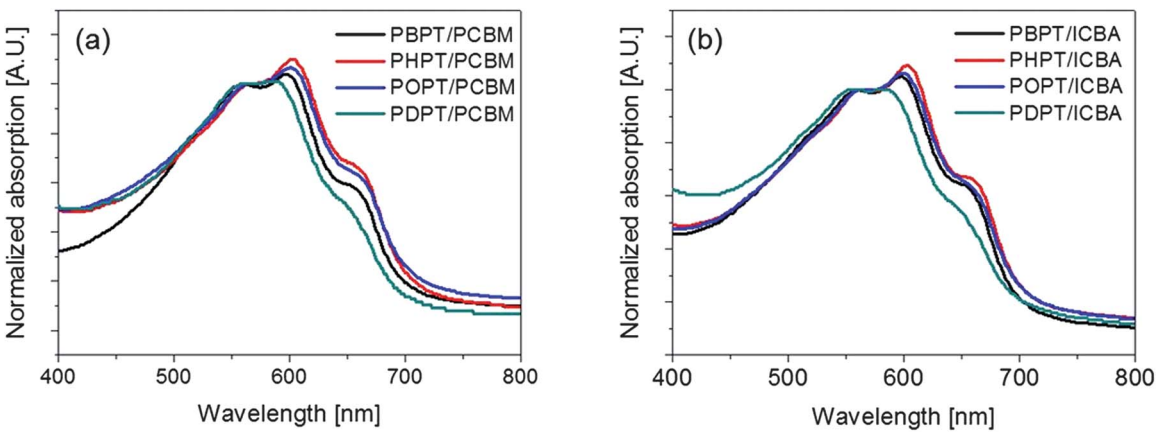

Fig. 6 UV-vis absorption spectra of (a) PAPT:PCBM and (b) PAPT:ICBA blend films under optimized device conditions.

Table 2 Optical properties of PAPT:PCBM and PAPT:ICBA blend films

	PAPT:PCBM			PAPT:ICBA		
	λ_{max} (nm)	I_{max}/I_{1st} [a]	I_{vib}/I_{1st} [b]	λ_{max} (nm)	I_{max}/I_{1st} [a]	I_{vib}/I_{1st} [b]
PBPT	596	1.04	0.59	598	1.05	0.64
PHPT	603	1.10	0.68	604	1.09	0.67
POPT	601	1.07	0.65	600	1.06	0.65
PDPT	588	1.01	0.52	587	1.00	0.57

[a] The relative intensity of maximum absorption peak (I_{max}) to first absorption peak (I_{1st}). [b] The relative intensity of vibronic peak (I_{vib}) to first absorption peak (I_{1st}).

with the first absorption peak at ~550 nm, were then calculated (Table 2). Regardless of the acceptor type, PHPT-based blend films show the most prominent vibronic features, indicating a higher order of crystallization; conversely, PDPT-based films exhibited vibronic peaks with reduced intensities and thus lower crystallization order. The addition of longer alkyl chains may disrupt the two-dimensional polymer packing and subsequent crystallization. The observed trend in the results is similar to that reported for P3AT systems.[19,29] We speculate that the reason for the weak vibronic features of PBPT is due to the extremely poor solubility of PBPT that may disturb the efficient packing of PBPT chains during the solution processing of films. Both intensity ratios (I_{max}/I_{1st} and I_{vib}/I_{1st}) increased in the same order as the device performance (in the decreasing order PHPT, POPT,

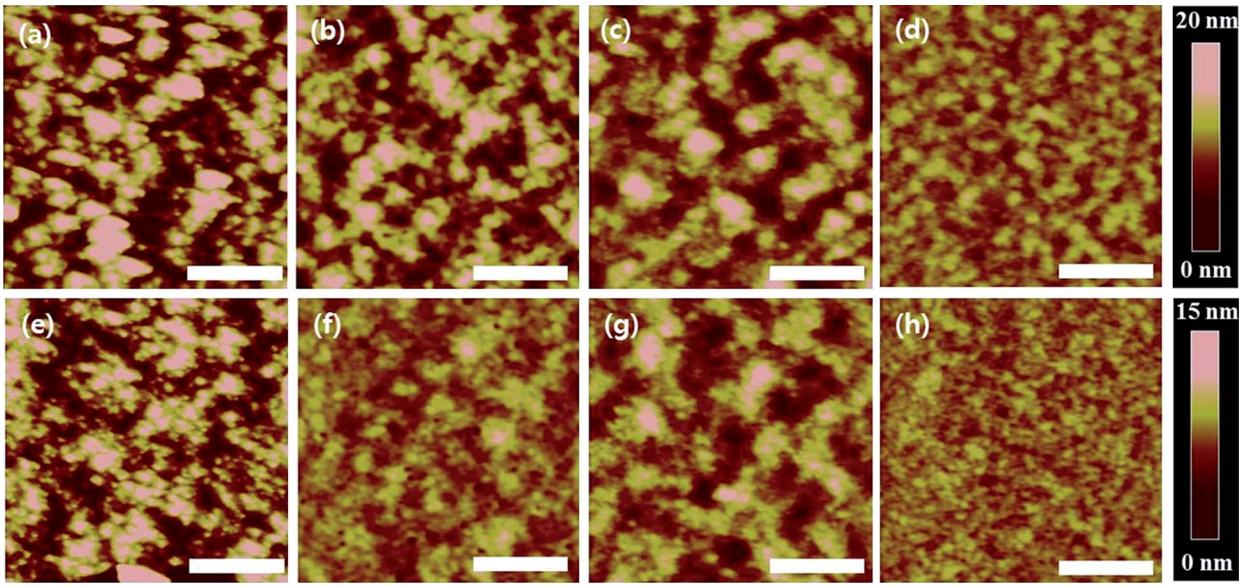

Fig. 7 Tapping-mode AFM topography images of PAPT:PCBM and PAPT:ICBA blend films: (a) PBPT, (b) PHPT, (c) POPT, and (d) PDPT blends with PCBM, (e) PBPT, (f) PHPT, (g) POPT, and (h) PDPT blends with ICBA. All samples were prepared under identical conditions to that for optimized devices. The scale bar is 1 μm. RMS roughness: (a) 4.3 ± 0.4 nm, (b) 3.2 ± 0.3 nm, (c) 2.8 ± 0.2 nm, (d) 1.4 ± 0.2 nm, (e) 3.4 ± 0.3 nm, (f) 1.2 ± 0.2 nm, (g) 1.8 ± 0.1 nm, and (h) 1.0 ± 0.4 nm.

PBPT and PDPT). Furthermore, the trend in λ_{max} for different PAPTs (in the decreasing order PHPT, POPT, PBPT and PDPT) is consistent with that of PCE. For this reason, the optical properties of PAPTs in the blend film could be one of the major contributions to the difference of the device performance as a function of side-chain length. In addition, the thin film optical absorption spectra of pristine PAPT films were measured for comparison (Fig. S4†). The change in the peak positions of PAPT films as a function of alkyl chain length is much less pronounced compared to that in the PAPT:acceptor blend films, indicating that the addition of PCBM or ICBA molecules in the PAPT blend films affects the packing structure of PAPT polymers. And, the interaction between the acceptor molecule and PAPT polymer is dependent on its alkyl chain length.

To gain deeper insight into the effect of alkyl chain length on the interaction between PAPT and electron acceptors, the nanoscale morphology of BHJ blend films was investigated using tapping-mode atomic force microscopy (AFM). Fig. 7 shows a series of AFM topography images of PAPT:PCBM (a–d) and PAPT:ICBA (e–h) blends, which were prepared under conditions identical to those used for optimized BHJ devices. The PAPT:ICBA blend films generally show lower root-mean-square (RMS) surface roughness than PAPT:PCBM blend films because of the intrinsically lower crystallinity of ICBA.[55] Regardless of the acceptor type, the RMS roughness was reduced with increasing alkyl chain length. PDPT:ICBA device shows the lowest RMS roughness among the different PAPT:PCBM and PAPT:ICBA devices. The trend of decreasing roughness with increasing alkyl side-chain length appears to be related to the increasing solubility of PAPTs with increasing side-chain length. The polymer with the longest alkyl chain (PDPT) retains better solubility as well as miscibility with fullerene acceptors, which results in smooth BHJ films. In contrast, poorly soluble PBPT begins to precipitate early in the spin-coating process while electron acceptors with relatively good solubility are precipitated at a much later stage. This unbalanced precipitation causes extensive phase separation and produces rough films. The inhomogeneous morphology of polymers with short alkyl chains provides a reasonable explanation for the lower PCE in PBPT-based systems: the inhomogeneous blend morphology reduces the interfacial area between electron donor and acceptor domains available for exciton dissociation and causes poor electrical contact between the active layer and cathode.

Conclusions

In this study, we demonstrated the correlation between PAPT alkyl chain length and BHJ photovoltaic device functions. Careful investigation of BHJ blend film properties was performed using four PAPTs with different alkyl chain lengths blended with PCBM or ICBA. While the optical properties of PAPT/electron acceptor films exhibit the strongest effect on the short-circuit current of the devices, a balance between the optical, electrical and morphological properties of PAPT:electron acceptor blend films caused by changes in the alkyl side-chain length was found to determine the overall photovoltaic performance of these devices. Among PAPTs, the hexyl group provides a good balance between crystallinity and miscibility with acceptors to achieve optimal optical properties and photovoltaic device performance. In addition, a bisadduct-type fullerene acceptor successfully enhanced the V_{oc} values and PCE of solar-cell devices. For example, PHPT:ICBA devices showed a PCE of 3.73%, which is the highest PCE for PAPT-based BHJ solar-cell devices reported thus far. GIXRD measurements revealed that the interlayer domain spacing of the PHPT is 2.51 nm, 0.86 nm longer than that of P3HT, which shows the best photovoltaic performance among P3ATs.

Acknowledgements

This research was supported by the Korea Research Foundation Grant funded by the Korean Government (2011-0030387, 2011-0010412), the New & Renewable Energy KETEP grant (2010-T100100460) and the Fundamental R&D Program Grant for Core Technology of Materials funded by the Ministry of Knowledge Economy Republic of Korea. Experiments at PLS were supported in part by MEST and POSTECH.

References

1 F. C. Krebs, *Sol. Energy Mater. Sol. Cells*, 2009, **93**, 394–412.
2 A. C. Arias, J. D. MacKenzie, I. McCulloch, J. Rivnay and A. Salleo, *Chem. Rev.*, 2010, **110**, 3–24.
3 B. C. Thompson and J. M. J. Fréchet, *Angew. Chem., Int. Ed.*, 2008, **47**, 58–77.
4 S. Gunes, H. Neugebauer and N. S. Sariciftci, *Chem. Rev.*, 2007, **107**, 1324–1338.
5 J. Peet, J. Y. Kim, N. E. Coates, W. L. Ma, D. Moses, A. J. Heeger and G. C. Bazan, *Nat. Mater.*, 2007, **6**, 497–500.
6 H. Zhou, L. Yang, A. C. Stuart, S. C. Price, S. Liu and W. You, *Angew. Chem., Int. Ed.*, 2011, **50**, 2995–2998.
7 H. Sirringhaus, P. J. Brown, R. H. Friend, M. M. Nielsen, K. Bechgaard, B. M. W. Langeveld-Voss, A. J. H. Spiering, R. A. J. Janssen, E. W. Meijer, P. Herwig and D. M. de Leeuw, *Nature*, 1999, **401**, 685–688.
8 R. J. Kline, M. D. McGehee, E. N. Kadnikova, J. S. Liu, J. M. J. Fréchet and M. F. Toney, *Macromolecules*, 2005, **38**, 3312–3319.
9 S. R. Scully and M. D. McGehee, *J. Appl. Phys.*, 2006, **100**, 034907.
10 X. N. Yang, J. Loos, S. C. Veenstra, W. J. H. Verhees, M. M. Wienk, J. M. Kroon, M. A. J. Michels and R. A. J. Janssen, *Nano Lett.*, 2005, **5**, 579–583.
11 J. S. Kim, Y. Lee, J. H. Lee, J. H. Park, J. K. Kim and K. Cho, *Adv. Mater.*, 2010, **22**, 1355–1360.
12 R. D. McCullough, R. D. Lowe, M. Jayaraman and D. L. Anderson, *J. Org. Chem.*, 1993, **58**, 904–912.
13 S. Rajaram, P. B. Armstrong, B. J. Kim and J. M. J. Fréchet, *Chem. Mater.*, 2009, **21**, 1775–1777.
14 Q. Peng, X. Liu, D. Su, G. Fu, J. Xu and L. Dai, *Adv. Mater.*, 2011, **23**, 4554–4558.
15 J. K. Park, J. Jo, J. H. Seo, J. S. Moon, Y. D. Park, K. Lee, A. J. Heeger and G. C. Bazan, *Adv. Mater.*, 2011, **23**, 2430–2435.
16 T. A. Chen, X. M. Wu and R. D. Rieke, *J. Am. Chem. Soc.*, 1995, **117**, 233–244.
17 V. Causin, C. Marega, A. Marigo, L. Valentini and J. M. Kenny, *Macromolecules*, 2005, **38**, 409–415.
18 B. C. Thompson, B. J. Kim, D. F. Kavulak, K. Sivula, C. Mauldin and J. M. J. Fréchet, *Macromolecules*, 2007, **40**, 7425–7428.
19 B. Friedel, C. R. McNeill and N. C. Greenham, *Chem. Mater.*, 2010, **22**, 3389–3398.
20 H. Bronstein, D. S. Leem, R. Hamilton, P. Woebkenberg, S. King, W. Zhang, R. S. Ashraf, M. Heeney, T. D. Anthopoulos, M. J. de and I. McCulloch, *Macromolecules*, 2011, **44**, 6649–6652.
21 H.-C. Chen, I. C. Wu, J.-H. Hung, F.-J. Chen, I. W. P. Chen, Y.-K. Peng, C.-S. Lin, C.-H. Chen, Y.-J. Sheng, H.-K. Tsao and P.-T. Chou, *Small*, 2011, **7**, 1098–1107.
22 Y.-W. Li, Y.-J. Chen, X. Liu, Z. Wang, X.-M. Yang, Y.-F. Tu and X.-L. Zhu, *Macromolecules*, 2011, **44**, 6370–6381.
23 S. Rathgeber, d. T. D. Bastos, E. Birckner, H. Hoppe and D. A. M. Egbe, *Macromolecules*, 2010, **43**, 306–315.
24 S. Rathgeber, J. Perlich, F. Kuehnlenz, S. Tuerk, D. A. M. Egbe, H. Hoppe and R. Gehrke, *Polymer*, 2011, **52**, 3819–3826.
25 H. Zhou, L. Yang, S. Xiao, S. Liu and W. You, *Macromolecules*, 2010, **43**, 811–820.
26 W. L. Ma, C. Y. Yang, X. Gong, K. Lee and A. J. Heeger, *Adv. Funct. Mater.*, 2005, **15**, 1617–1622.
27 G. Li, V. Shrotriya, J. S. Huang, Y. Yao, T. Moriarty, K. Emery and Y. Yang, *Nat. Mater.*, 2005, **4**, 864–868.
28 G. Q. Ren, P. T. Wu and S. A. Jenekhe, *Chem. Mater.*, 2010, **22**, 2020–2026.
29 L. H. Nguyen, H. Hoppe, T. Erb, S. Gunes, G. Gobsch and N. S. Sariciftci, *Adv. Funct. Mater.*, 2007, **17**, 1071–1078.
30 W. D. Oosterbaan, J. C. Bolsee, A. Gadisa, V. Vrindts, S. Bertho, J. D'Haen, T. J. Cleij, L. Lutsen, C. R. McNeill, L. Thomsen, J. V. Manca and D. Vanderzande, *Adv. Funct. Mater.*, 2010, **20**, 792–802.
31 H. Xin, F. S. Kim and S. A. Jenekhe, *J. Am. Chem. Soc.*, 2008, **130**, 5424–5425.
32 A. Gadisa, W. D. Oosterbaan, K. Vandewal, J. C. Bolsee, S. Bertho, J. D'Haen, L. Lutsen, D. Vanderzande and J. V. Manca, *Adv. Funct. Mater.*, 2009, **19**, 3300–3306.
33 P. T. Wu, G. Q. Ren, C. X. Li, R. Mezzenga and S. A. Jenekhe, *Macromolecules*, 2009, **42**, 2317–2320.
34 M. H. Chen, J. Hou, Z. Hong, G. Yang, S. Sista, L. M. Chen and Y. Yang, *Adv. Mater.*, 2009, **21**, 4238–4242.
35 A. P. Zoombelt, M. A. M. Leenen, M. Fonrodona, Y. Nicolas, M. M. Wienk and R. A. J. Janssen, *Polymer*, 2009, **50**, 4564–4570.
36 L. Biniek, S. Fall, C. L. Chochos, D. V. Anokhin, D. A. Ivanov, N. Leclerc, P. Leveque and T. Heiser, *Macromolecules*, 2010, **43**, 9779–9786.
37 M. Granstrom, K. Petritsch, A. C. Arias, A. Lux, M. R. Andersson and R. H. Friend, *Nature*, 1998, **395**, 257–260.
38 T. W. Holcombe, C. H. Woo, D. F. J. Kavulak, B. C. Thompson and J. M. J. Fréchet, *J. Am. Chem. Soc.*, 2009, **131**, 14160–14161.
39 T. W. Holcombe, J. E. Norton, J. Rivnay, C. H. Woo, L. Goris, C. Piliego, G. Griffini, A. Sellinger, J. L. Bredas, A. Salleo and J. M. J. Fréchet, *J. Am. Chem. Soc.*, 2011, **133**, 12106–12114.
40 C. H. Woo, T. W. Holcombe, D. A. Unruh, A. Sellinger and J. M. J. Fréchet, *Chem. Mater.*, 2010, **22**, 1673–1679.
41 C.-H. Cho, H. Kang, T. E. Kang, H.-H. Cho, S. C. Yoon, M.-K. Jeon and B. J. Kim, *Chem. Commun.*, 2011, **47**, 3577–3579.
42 G. J. Zhao, Y. J. He and Y. F. Li, *Adv. Mater.*, 2010, **22**, 4355–4358.
43 Y. J. He, H. Y. Chen, J. H. Hou and Y. F. Li, *J. Am. Chem. Soc.*, 2010, **132**, 1377–1382.
44 K.-H. Kim, H. Kang, S. Y. Nam, J. Jung, P. S. Kim, C.-H. Cho, C. Lee, S. C. Yoon and B. J. Kim, *Chem. Mater.*, 2011, **23**, 5090–5095.
45 Z.-L. Guan, J. B. Kim, Y.-L. Loo and A. Kahn, *J. Appl. Phys.*, 2011, **110**, 043719–043715.
46 N. C. Miller, S. Sweetnam, E. T. Hoke, R. Gysel, C. E. Miller, J. A. Bartelt, X. Xie, M. F. Toney and M. D. McGehee, *Nano Lett.*, 2012, **12**, 1566–1570.
47 M. Jeffries-El, G. Sauve and R. D. McCullough, *Macromolecules*, 2005, **38**, 10346–10352.
48 H. Kang, C. Lee, S. C. Yoon, C.-H. Cho, J. Cho and B. J. Kim, *Langmuir*, 2010, **26**, 17589–17595.
49 B. J. Kim, Y. Miyamoto, B. W. Ma and J. M. J. Fréchet, *Adv. Funct. Mater.*, 2009, **19**, 2273–2281.
50 C. H. Woo, B. C. Thompson, B. J. Kim, M. F. Toney and J. M. J. Fréchet, *J. Am. Chem. Soc.*, 2008, **130**, 16324–16329.
51 H. J. Kim, A. R. Han, C.-H. Cho, H. Kang, H.-H. Cho, M. Y. Lee, J. M. J. Fréchet, J. H. Oh and B. J. Kim, *Chem. Mater.*, 2012, **24**, 215–221.
52 E. J. Zhou, Z. Tan, C. H. Yafng and Y. F. Li, *Macromol. Rapid Commun.*, 2006, **27**, 793–798.
53 H. Azimi, A. Senes, M. C. Scharber, K. Hingerl and C. J. Brabec, *Adv. Energy Mater.*, 2011, **1**, 1162–1168.
54 M. A. Faist, T. Kirchartz, W. Gong, R. S. Ashraf, I. McCulloch, J. C. de Mello, N. J. Ekins-Daukes, D. D. C. Bradley and J. Nelson, *J. Am. Chem. Soc.*, 2011, **134**, 685–692.
55 H. Kang, C.-H. Cho, H.-H. Cho, T. E. Kang, H. J. Kim, K.-H. Kim, S. C. Yoon and B. J. Kim, *ACS Appl. Mater. Interfaces*, 2012, **4**, 110–116.